Scientific Research Publishing

Open Journal of Optimization, 2025, 14(4), 147-180
https://www.scirp.org/journal/ojop
ISSN Online: 2325-7091
ISSN Print: 2325-7105

Evaluating Physico-Mechanical Behaviour of Pyrethrum Using Principal Component Analysis and Response Surface Modeling for Optimal Design and Performance of Precision Harvesters

Andrew Mwamba[1*], Frankline Mwiti[1,2], Solomon Mulindi[1]

[1]Department of Agricultural and Biosystems Engineering, University of Eldoret, Eldoret, Kenya
[2]Department of Environmental and Biosystems Engineering, Machinery Section, University of Nairobi, Nairobi, Kenya
Email: *andrew.mwamba@uoeld.ac.ke

How to cite this paper: Mwamba, A., Mwiti, F. and Mulindi, S. (2025) Evaluating Physico-Mechanical Behaviour of Pyrethrum Using Principal Component Analysis and Response Surface Modeling for Optimal Design and Performance of Precision Harvesters. *Open Journal of Optimization*, **14**, 147-180.
https://doi.org/10.4236/ojop.2025.144009

Received: August 25, 2025
Accepted: November 23, 2025
Published: December 1, 2025

Abstract

Pyrethrum (*Chrysanthemum cinerariaefolium* L.) is an industrial crop with complex morphology and diverse physico-mechanical properties that jeopardize the optimal design of precision harvesters. This study adopted multivariate correlation, Principal component analysis (PCA) and Response surface methodology (RSM) to characterize mechanistic relationships among morpho-physio-mechanical properties of pyrethrum plant to optimize design and performance of precision harvesters. Mature stalks were established in a completely randomized design of three (3) diverse field sites, with triplications (3) in Kenya's Nakuru, Uasin Gishu, and Kericho counties, under irrigated and rainfed agriculture. Results showed that all bio-physical-mechanical parameters had bell-shaped frequency distribution, indicating generalized normality and good statistical range for adoption in mechanized harvesters. Multivariate analysis revealed a strong positive correlation (0.91) of wet floral unit volume (V_f) with unit floral mass (*MIF*). In contrast, floral diameter (*FD*) with porosity (Φ), and dry floral volume (V_d) with volumetric coefficient of expansion (Ψ_v) had the most significant negative correlation (−0.98). However, MIF with shoot internode length (*SIL*), actual density (ρ_t) with MIF, biomass repose angle (θ) with floral head diameter (*FHD*), θ with ρ_b, shear strength (τ) with *FD*, and Ψ_v with bulk porosity (ε), respectively, were uncorrelated (0.0). Cutting resistance force (R_c), plucking force (F_p), and mechanical compressibility (c) were non-linearly correlated. First-order linear model characterized the relationship between R_c, moisture content (*MC*), and mature stalk height (*MSH*).

The first-order regression model best described V_d as a function of Ψv and V_f. The first-order surface response model also characterized *MSH*, flower canopy width (*FCW*), and *SIL*. Second-order surface response characterized F_p, R_c, and $\acute{c}$ forces during mechanized harvesting. Further, a downward second-order open parabola characterized R_c, *MC*, and F_p, and their optimal response model was curvilinearly quadratic. However, *MC*, τ, and *FD* were asymmetrically curvilinear but revealed a second-order surface. Lowest τ values occurred at high *MC* and lowest *FD*. All bio-physical-mechanical characteristics of pyrethrum significantly ($p < 0.01$) affect the design of precision harvesters.

Keywords

Pyrethrum Mechanization, Multivariate Analysis, Quadratic Curvilinear Model, Repose Angle, Plucking Force, Mechanical Compressibility, Shear Strength, Sphericity

1. Introduction

Pyrethrum (*Chrysanthemum cinerariaefolium* L.) is grown for its daisy-like and whorled white ray of flowers with a yellow centre head containing natural pyrethrin insecticide. The botanical pyrethrin is competitive with synthetic insecticides due to its selective toxicity and lower environmental hazards [1]. Mature pyrethrum flowers contain 94% of pyrethrin, while 6% is contained in other parts of the plant [2]. The complex physio-morphological structure of the crop demands selective harvesting because only the mature achenes within the flower head contain the pyrethrin [3], making it the only prime target during harvesting. As such, only the mature flowers are picked during harvesting for further separation and processing. Furthermore, as a perennial ratoon crop, pyrethrum produces flower-bearing stalks that mature at different stages, complicating mechanized harvesting. Variations in growth, ratooning, stalk maturity, and various flower blooming stages jeopardise the optimal design of precision harvesters. Small and medium-scale pyrethrum harvesting has thus been performed manually through hand picking, as illustrated in **Figure 1**.

Figure 1. Handpicking for selective harvesting of mature pyrethrum flowers.

Although much literature is available on the occurrence and accumulation of pyrethrin in mature flowers, there is only a limited understanding of the morphological factors of the pyrethrum plant and how they would influence the design of mechanized precision harvesters. According to [4], studying biophysical-mechanical, morpho-mechanical, and rheological parameters of complex plant materials is pertinent for accurate simulations and agricultural process equipment design. A database of actual morphological and physico-mechanical properties of the pyrethrum plant and flowers is critical in guiding the modern design for precision harvesters. However, empirical methods utilized by olden day engineers become time-consuming and increase development costs. As such, morpho-physical, rheolo-mechanical, crop dimensions and geometry, conveyance and flow characteristics have been the thrust of all precision harvesting machinery designers [4] [5]. For instance, plant mechanical properties shearing force (ν) shear strength (τ) and tensile stress (σ) are necessary for the design of cutting and shear parts, conveying surfaces, threshing units and plucking mechanisms and for determination of cutting angles, speed and velocities, energy requirements and wear resistance [6]-[10]. At the same time, physio-morphological crop parameters provide essential criteria for the mechanical design of harvester structure and the key components of the entire crop-machine interaction interface [4]. For instance, stem diameter and moisture content influence static and dynamic cutting forces [11]. Among other biophysical-mechanical properties of crops, cutting forces, shear strength, and picking forces influence energy requirements during harvesting and can guide the selection of force response units and operational parameters [12]. Other factors affecting the design of field crop harvesting machines include crop moisture content at harvest, stem diameter, shear strength, cutting speed, and bulk volumetric feed rates [13]-[15]. Previous researchers have reported morpho-physical structure, rheological and mechanical properties of other field crops for design and development of mechanized harvesters including sunflower [16], barley [17], paddy rice [18], wheat [19] [20], carrots [21] [22], green leafy vegetables [23] and fruits such as tomatoes [24] [25], chillies [26], and strawberry [27]. However, critical bio-physical, morpho-mechanical, and rheological parameters of mature pyrethrum plants and flowers that would guide the design of precision harvesters are missing in the literature.

Due to variations in the stages of growth and ratooning, stalk maturity, flower head ripening stages, and the complex morphological architecture, mechanizing the morphological parameters for designing medium and small-scale mechanized precision harvesters is challenging. Further, the Morphological and physio-mechanical plant characteristics of mature pyrethrum stalks are variable within the fields, thus complicating process design and the selective mechanism of precision harvesting. Therefore, pyrethrum harvesting resorts to manual selection and hand picking of mature flowers, which is currently the most time and labor-consuming operation in pyrethrum production [28] [29]. Furthermore, manual handpicking during harvesting exposes workers to allergic health hazards associated with pyrethrin [30]. Owing to scanty literature on developing precision pyrethrum har-

vesters, this study examines pyrethrum flower (Figure 2) and plant parameters relevant for precision design and performance optimization of small-scale mechanized pyrethrum harvesters.

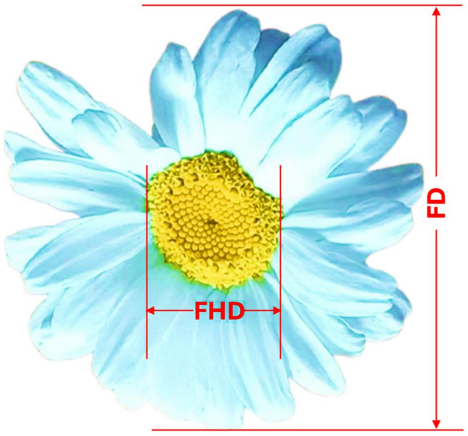

Figure 2. Pyrethrum flower parameters for design of precision harvesters.

The study aims at establishing morphological parameters, viz, mature stalk height (*MSH*), shoot diameter (*SD*), shoot internode length (*SIL*), floral diameter (*FD*), floral head diameter (*FHD*), floral peduncle length (*FPL*), flower canopy width (*FCW*), and floral peduncle diameter (*FPD*). Bio-physical properties included, moisture content (*MC*), bulk density (ρ_b), Porosity (Φ) of, actual density (ρ_t), bulk porosity (ε), unit floral mass (MIF) wet floral unit volume (V_f), dry floral volume (V_d), Volumetric coefficient of expansion (Ψ_v), sphericity (φ) and biomass repose angle (θ) while rheolo-mechanical properties included shear strength (τ), tensile strength (σ), plucking force (F_p), repose angle (θ), kinetic friction (μ_K), and static friction modulus (μ_S), compressed density (ρ_c), cutting resistance force (R_c), compressed density (ρ_c) and mechanical compressibility ($\acute{c}$). Therefore, the study was designed to (i) characterize the morphological, physico-mechanical, and rheological properties of mature pyrethrum stalks and flowers across diverse Kenyan field sites, (ii) apply principal component analysis (PCA) to reduce dimensionality and identify key plant traits influencing harvester design; (iii) employ response surface methodology (RSM) to develop predictive models of critical harvesting parameters; and (iv) translate these analytical findings into practical engineering insights for optimizing small-scale precision pyrethrum harvester components.

2. Materials and Methods

2.1. Experimental Sites and Sampling Design

Field investigations were conducted in the pyrethrum fields of Lanet in Nakuru county (0˚19'29.66" S, 36˚12'21.19" E), Moiben in Uasin Gishu county (0˚34'15.8" N, 35˚18'31.1" E), and Turi in Kericho county (0˚16'28.7" S, 35˚46'30.9" E) in Kenya, as shown in Figure 3.

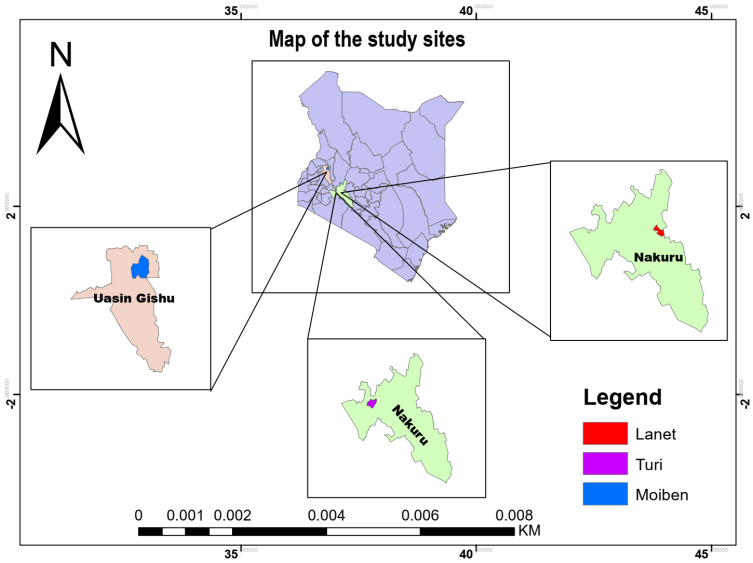

Figure 3. Map of the study areas and sampling sites.

Mature pyrethrum flower stalks were randomly identified and tagged from a completely randomized experimental net plot measuring (100 × 100 m^2) isolated in 4 quadrants of the field sites measuring 40,000 m^2 with triplications. The sample size was established from a random sampling technique using Equation (1) [31] [32].

$$n = \frac{N}{1 + N\left(\alpha^2\right)} \tag{1}$$

where n, N, and α are the sample size, total population, and significance levels (0.05), respectively.

2.2. Determination of Morphological Parameters

Dimensions of seven morphological parameters, including *MSH*, *SD*, *SIL*, *FD*, *FHD*, *FPL*, and *FPD*, were established for each of the 10 plants in the field using digital vernier and measuring tape (**Figure 4**). Each of the readings was then summed up to establish the average values for each parameter in each quadrant and the entire field.

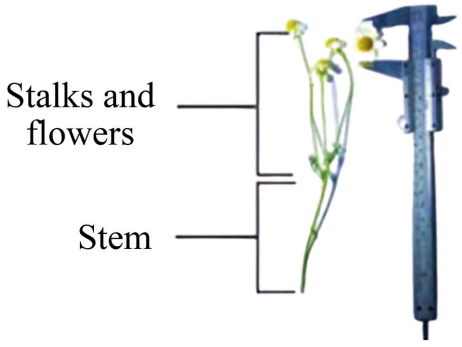

Figure 4. Measurement of various pyrethrum flower stalk dimensions.

2.3. Determination of Bio-Physical Properties of Pyrethrum Stalks

Crop samples were collected in the respective isolations above and referenced for laboratory and testing of moisture content (MC), bulk density (ρ_b), and Porosity (Φ) of mature pyrethrum flowers.

2.3.1. Determination of Moisture Content of Mature Pyrethrum Stalks

Moisture content (MC) of mature pyrethrum flower stalk influences its size, volume, shear stiffness and strength, plucking energy, and cutting force. Pyrethrum flowers were isolated from each experimental site and placed in airtight containers to prevent moisture fluctuations. In the laboratory, three samples from each experimental site were sequentially placed on the biomass sample pans and placed in a controlled moisture balance drying chamber until there was no further drop in weight. The procedure was triplicated to obtain average results. Thereafter, MC was established as a percentage of total pyrethrum stalk weight using Equation (2) [33] [34].

$$MC = \frac{m_{if} - m_f}{m_i} \times 100\% \tag{2}$$

where m_{iw} is the initial floral unit mass and w_f is the final constant mass of pyrethrum stalk after drying.

2.3.2. Determination of Bulk Density and True Density

Flower mass and compressed densities impact crop handling component designs of pyrethrum harvesters by influencing volumetric performance, flexibility, or weight reduction of handling components. The bulk density (ρ_b) of pyrethrum flower stalk sample was determined as the ratio of the weighted mass of the sample (m_s) to its total hectoliter tester volume (v_h) using Equation (3) [35].

$$\rho_b = \frac{m_s}{v_h} \tag{3}$$

The actual density (ρ_t) of pyrethrum flower stalks was determined using a pycnometer density cup of 61 g with a calibrated volume of 50 ml that was cleansed, filled with flower stalks, placed in an analytical electronic balance (0.0001 g), and its weight recorded after stabilizing, with triplications. The ρ_t of pyrethrum flower stalk samples was then determined as the ratio of weighted sample mass to its total pycnometer displacement volume using Equation (4) [33] [36].

$$\rho_t = \frac{m_{sc} - m_c}{v_c} \tag{4}$$

where m_{sc} is the total weight of the sample and pycnometer density cup, while m_c and v_c are the weight and volume of the pycnometer, respectively.

2.3.3. Determination of Bulk Porosity

The bulk porosity (ε) of the pyrethrum flower biomass superficially affects bulk density, the amount of flower biomass handled, harvesting feed rate, material flow, and efficiency of conveying cut material. Pyrethrum ε was defined by the

fraction of the spaces within the bulk flower stalk, not occupied by the flowers. From the electronic balance and the pycnometer displacement method, the ε of flowers was determined using Equation (5) [35] [37].

$$\varepsilon = \left(1 - \frac{\rho_b}{\rho_t}\right) \times 100 \tag{5}$$

2.3.4. Floral Unit Volume

The floral unit volume (V_f) affects the component space and size design for accurate separation and precision handling during selective flower-biomass harvesting. The volume (V_f) of pryrethrum flowers was established by relating the unit mass (m) of flowers used in the computation of true density using Equation (6) [35].

$$V_f = \frac{m}{\rho_t} \tag{6}$$

where m is the unit wet mass of pyrethrum flowers measured using an electronic balance with 0.001 g sensitivity.

2.3.5. Volumetric Coefficient of Expansion

Volumetric coefficient of expansion (Ψ_v) of pyrethrum impacts precision harvester component dimensions and cutting forces. Higher Ψ_v induces higher cutting forces potentially requiring the design of a high-strength cutting potentially requiring the design of a high-strength cutting mechanism. Volumetric coefficient of expansion (Ψ_v) of pyrethrum was determined using Equation (7) [35].

$$\Psi_v = \frac{V_f}{V_d} \tag{7}$$

where V_d is the experimental dry unit volume of the flower.

2.3.6. Determination of Sphericity

The degree to which irregularly shaped pyrethrum flower stalks resemble a sphere impacts their flowability behavior on contact equipment surfaces. It also determines friction resistance, interlocking and surface adhesion interactions, and the final design of cutting and conveying surfaces. Higher sphericity values (closer to 1) improve flowability, while lower values result in difficult flow handling. Pyrethrum floral sphericity (φ) was determined by relating equivalent diameter with floral head length (L) using Equation (8) [38].

$$\varphi = \frac{\left(6v_f/\pi\right)^{-3}}{L} \tag{8}$$

2.3.7. Repose Angle of Flower Biomass

The dynamic angle of repose (θ) on a surface enables assessment of the interaction between pyrethrum flower biomass with different angular surfaces, providing insights into their handling, transport, and flow properties, and giving valuable information to the design of precise transportation, conveying, and handling mechanisms. A fixed base (piling method) was used to determine θ for

pyrethrum. Mature stalks containing the flower heads were poured into a conical heap; the height (h) of the free surface and the base diameter (d) of the formed cone pile were measured. The θ for pyrethrum was thereafter computed using Equation (9) [33].

$$\theta = \tan^{-1}\left(\frac{2h}{d}\right) \tag{9}$$

where h is the height of the free surface (cm), and d is the cone pile diameter (cm).

2.4. Mechanical Properties of Pyrethrum Plant

Crop samples were collected in the above-referenced isolates for laboratory and testing of 6 rheological-mechanical parameters. These included shear strength (τ), tensile strength (σ), static friction modulus (μ_s), compressed density (ρ_c), and mechanical compressibility (c). Because some of the mechanical tests, such as tensile tests, cannot be utilized to test all types of crop stalk samples, clamp stretching methods for mechanical tests of biological plant materials was designed and improvised as recommended for crop-specific applications [4] [39] [40].

2.4.1. Determination of Tensile Strength and Plucking Force

Tensile force is a fundamental parameter for determining the tension forces required to break the flower component from stalks during precision plucking in mechanized pyrethrum harvesters. Both tensile strength (σ) and plucking force (F_P) influence the physico-mechanical properties of pyrethrum flowers that affect harvesting components. A custom-built measurement apparatus was developed, using a high-precision digital electronic measurement (±0.001 kg), mounted vertically for plucking stress measurement, integrated with three structural plates (upper, middle, and base) supported by a square hollow section tube for stem stability during loading. Pyrethrum stems of various diameters and containing flowers of different sizes were coupled at the tensioning end of the load cell using a diameter rubber ring, for consistent and repeatable gripping, and subjected to uniform tensile load. At the same time, the yielding force was recorded by the locking load cell to establish σ and thereafter decoupled.

2.4.2. Determination of Shear Strength

Pyrethrum shear strength (τ) guides the determination of cutting forces and mechanisms and is a critical parameter in designing and optimizing the performance of precision harvesting systems. The upper limits of τ provide the maximum shear stress that the flower peduncle and floral stalk base of pyrethrum can withstand before shear failure during harvesting [41]. The τ of pyrethrum stalks is a critical characterization variable for mechanized precision harvesting. Multiple flower samples ($n \geq 5$) from all the sites were obtained, and flower peduncle diameters were measured using a micrometer and mounted in a horizontal shear fixture of a shear blade. Shear force was then induced by the Load cell at a constant speed of 5 mm/min until failure. The failure point peak force and cross-sectional area (A) at failure were established, and the τ was calculated

using Equation (10) [41].

$$\tau = \frac{F}{A} \text{ and } A = \pi \frac{d^2}{4} \tag{10}$$

where τ, F, and A are the shear strength ($N \cdot Nm^{-2}$), Force at failure point (N), and the shear plane Area (m^2), respectively.

2.4.3. Determination of Net Shear Force, Shear Stress and Specific Shear Energy

A quasi-static pivoted double shear scissor test rig was constructed using a pivoted scissor-shear mechanism coupled with a calibrated tension thread to measure the effective shear force (σ_n) resisted by pyrethrum stalk to cutting force at a 45˚ sharpened edge angle. Shear force (F_T) for all the isolated flower stalks was obtained, and the average force was determined by measuring F_T and scissor mechanism force (F_α) and used to compute effective σ_n using Equation (11) [4] [19] [42].

$$\sigma_n = F_T - F_\alpha \tag{11}$$

where σ_n, F_T, and F_a are the net/effective shear force (N), measured shear force (m.g) in N, and the scissor force (N) divided by 2, respectively, m being the mass and g is 9.81 m/s^2. The F_a was computed as half of the scissor geometry reaction force using Equation (12) [19] [42].

$$F_\alpha = \frac{1}{2} \text{m.g} \tag{12}$$

The respective shear stress (Ss) and specific shear energy (SE_s) were then determined using Equation (13) and Equation (14) [4] [19] [42].

$$Ss = \frac{F_s}{2A_s} \tag{13}$$

$$SE_s = \frac{SE}{2As} \tag{14}$$

where Ss and F_s are the shear stress and force at failure, while A_s, SE_s, and SE are the respective sample notch area (m^2), shear, and specific shear energies at failure (kN·m).

2.4.4. Determination of Cutting Resistance Force

The shear cut method was used to obtain the cutting resistance force (R_C) of pyrethrum flower stalks by pulling a digital scale to read the cutting load of the shear-cut-scissor mechanism, as shown in **Figure 5**. The cutting load is converted to force by multiplying by g. The cutting resistance was then calculated using Equation (15) [43].

$$R_C = \frac{W\left(CA + \frac{SD}{2}\right)}{F_A} \times g \tag{15}$$

where R_c is the cutting resistance force (N), W is the measured weight (kg), CA is the cutting arm (m), SD is the shoot stem diameter and F_A is the force arm.

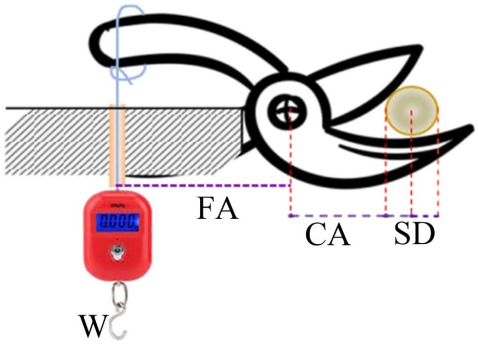

Figure 5. Schematic determination of pyrethrum stalk cutting resistance forces.

2.4.5. Determination of Static Friction Modulus

The static friction modulus coefficient (μ_S) of pyrethrum flowers guides the selection criterion of crop-machine interaction surfaces and their flow and durability assessment. The μ_S of pyrethrum flowers was determined for four different surface materials: galvanized sheet, stainless steel (grade 304), rubber, and plywood. The flowers were aligned parallel to the direction of motion during testing. A four-sided plywood container, measuring 1.00 m × 0.35 m × 0.40 m and open at both ends, was used for the experiment. The tangent of the inclination angle was measured using a graduated scale, and μ_S was calculated using Equation (16) [37].

$$\mu_S = \tan\beta \tag{16}$$

where μ_S and β are the static friction coefficient and the inclination angle respectively.

2.4.6. Compressed Density and Mechanical Compressibility

The compressed density (ρ_c) of pyrethrum flower-stalks determines bulk flower flow in compressed feedstock states and was calculated using the relationship in Equation (17) [37]

$$\rho_c = m_f \times V_t^{-1} \tag{17}$$

where m_f and V_t are the flower mass and true volume occupied by the flowers. Further, the mechanical compressibility ($\acute{c}$) defined as the change in bulk density upon consolidation force was established as the ratio of change in volume under compression of bulk flower material using Equation (18) [44].

$$\acute{c} = \frac{V_o - V_c}{V_o} \times 100 = 1 - \frac{\rho_o}{\rho_c} \tag{18}$$

where V_o and ρ_o are the initial volume and bulk density, while V_c and ρ_c are the final compressed volume and bulk density of the flower-stalk sample, respectively.

2.5. Statistical Analysis

2.5.1. Multivariate Correlation

Correlation analysis was performed to establish the presence or absence of statistical relationships between morpho-physical and rheological-mechanical var-

iables of pyrethrum. Spearman's rank correlation was used to assess monotonic associations between mechanical harvesting force and morphological characteristics. This non-parametric measure is appropriate when data violate normality assumptions and are prone to outliers [45] [46]. Scatterplots were established to determine non-linearities and monotonic trends [47], using the ccomputation function cor(), in *R*, with method set to "spearman", and exact p-values were obtained via 10,000 permutation resamples to improve inference stability. Tied ranks were handled automatically, and significance levels were assessed at α = 0.05, while Spearman's rank correlation coefficient was determined using Equation (19) [48]-[50]. All computations were performed in statistical software *R* (v4.4).

$$r_s = 1 - \frac{6\sum d_i^2}{n\left(n^2 - 1\right)} \tag{19}$$

where d_i is the difference between the ranks of each observation.

2.5.2. Principal Component Analysis

Principal Component Analysis (PCA) was employed to reduce the high dimensionality of measured pyrethrum traits and identify the most influential variables for mechanized harvesting. PCA is widely applied in agricultural engineering to reduce trait complexity and extract latent factors that underpin plant-machine interactions, thereby enabling more targeted design decisions [51] [52].

The PCA was adopted to explore the multivariate dynamics of diverse sets of morphological, mechanical, and physical traits measured in floral biomass. PCA is a mathematically robust, unsupervised machine learning method for identifying dominant patterns in high-dimensional data. It provides a set of uncorrelated latent variables (principal components) that explain the most variance, enabling compression, visualization, and preprocessing for downstream tasks. PCA analysis aimed to reduce dimensionality, identify patterns of trait association, and provide insights relevant to design considerations of mechanized harvesters. First, the covariance matrix was computed using Equation (20) [53].

$$\sum = \frac{1}{n-1} X^T X \tag{20}$$

where, X is the centered data matrix with n observations and s variables. The eigenvalue problem solved using Equation (21) [53].

$$\sum v = \lambda \cdot v \tag{21}$$

where λ is the Lagrange multiplier of the eigen vector v. The eigenvectors v_i are the principal axes, while the eigenvalues λ_i indicate the explained variance. The principal component was finally obtained using Equation (22) [54].

$$PC_1 = X_{w1} \tag{22}$$

where PC_1 is the direction of maximum variance in the data and w_1 is the eigenvector of Σ with the largest eigenvalue.

3. Results and Discussion

3.1. Prevalence and Distribution of Morpho-Physical and Rheolo-Mechanical Variables

The distribution and range of occurrence of all morphological and physio-mechanical pyrethrum variables pertinent to the design of precision harvesters are shown in Figure 6. The pattern of frequency distribution generally revealed a bell-shaped curve, indicating a normally distributed range of all pyrethrum plant variables for generalized adoption in further analysis that guides the design of precision harvesters. Higher frequencies indicated greater prevalence in all fields, while lower frequencies suggested that the variable was less common.

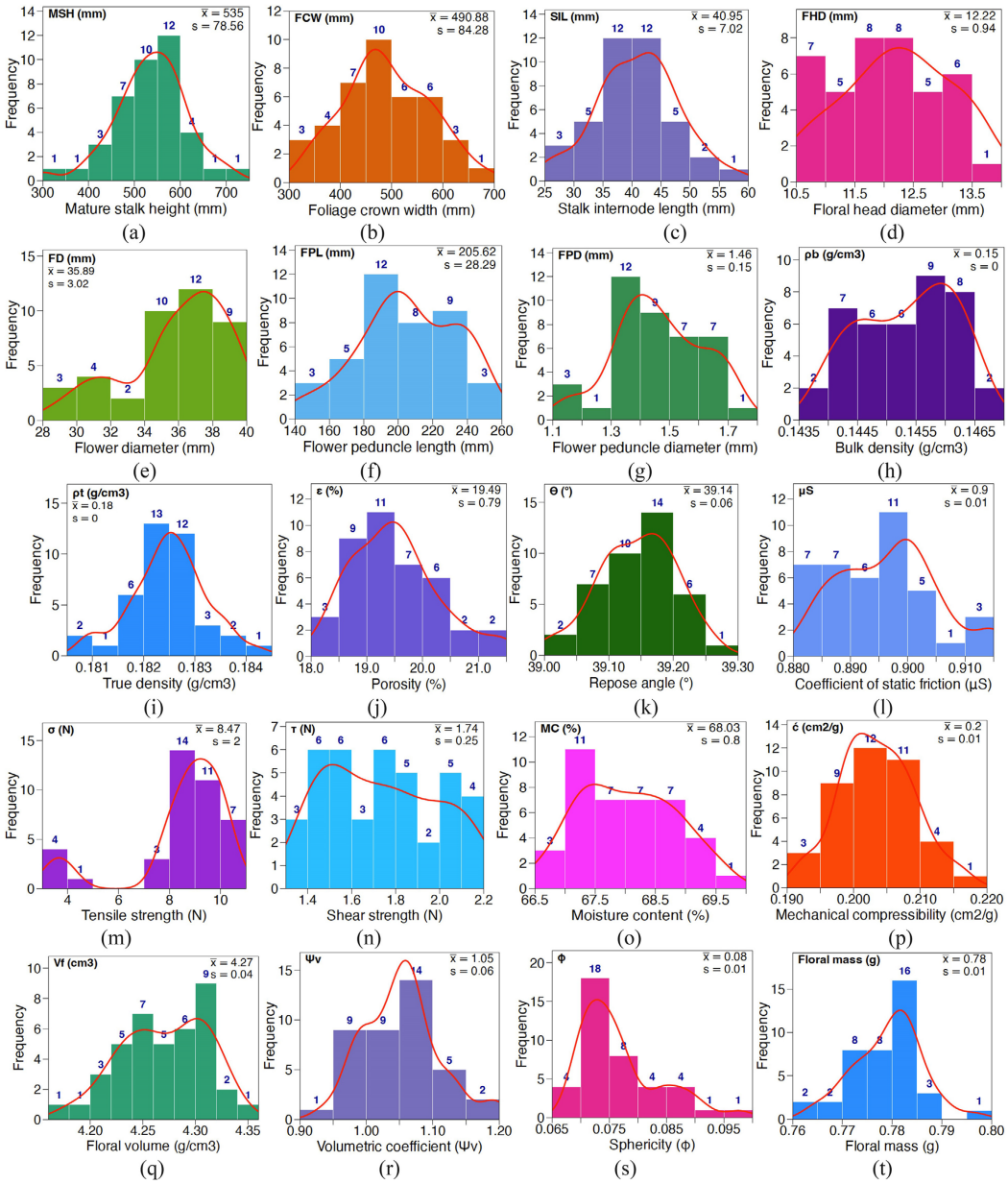

Figure 6. Distribution of morpho-physical and rheolo-mechanical traits of pyrethrum across sites.

3.2. Multivariate Correlation among Pyrethrum Plant Variables

Correlation analysis of relationships among pyrethrum plant variables is shown in the correlation matrix (Figure 7). The FD with Φ and V_d with Ψ_v had the most significant negative correlation (−0.98). At the same time, V_f with MIF demonstrated the highest positive correlation (0.91), while MIF with SIL, ρ_t with MIF, θ with FHD, θ with ρ_b, τ with FD, and Ψ_v with ε, respectively, did not correlate (0.0).

3.3. Principal Component Analysis and Evaluation

The PCA revealed five principal components (PCs) with eigenvalues greater than one, as shown in Table 1, which cumulatively explained 70.96% of the total variance in the pyrethrum biophysical-mechanical properties. This suggests that a substantial proportion of the original trait variability can be interpreted using a limited number of uncorrelated axes, thus simplifying and reducing trait analysis and visualization for machinery design.

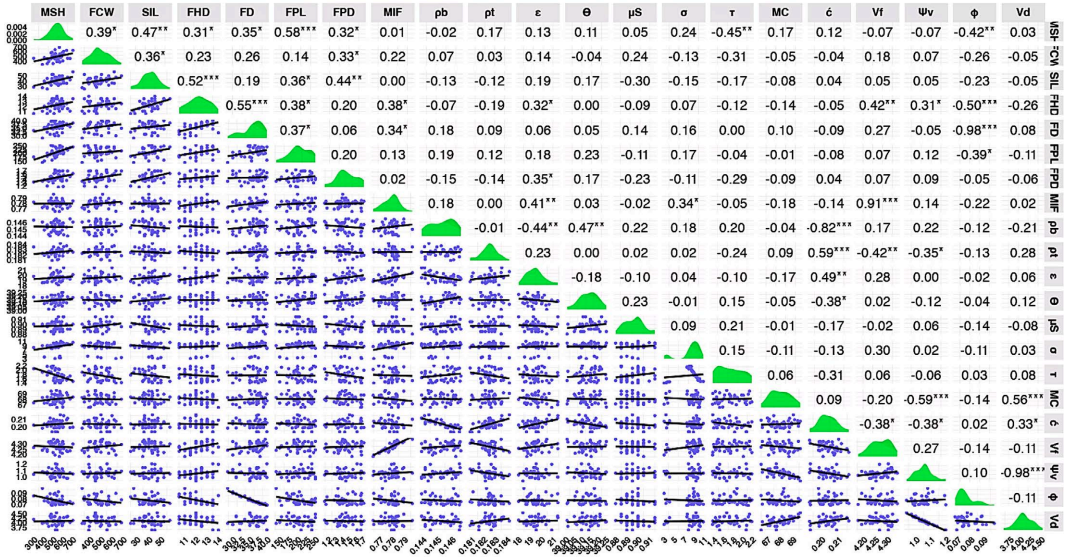

Figure 7. Multivariate correlation among mature pyrethrum plant variables.

Table 1. Principal components explaining the variance of pyrethrum parameters.

PC	Eigenvalue	% Variance	Cumulative %
PC1	3.200*	26.667	26.667
PC2	1.693*	14.108	40.775
PC3	1.285*	10.709	51.483
PC4	1.232*	10.265	61.748
PC5	1.105*	9.211	70.959
PC6	1.039*	8.659	79.617
PC7	0.641	5.344	84.961
PC8	0.581	4.844	89.806

Continued

PC9	0.507	4.222	94.027
PC10	0.352	2.934	96.961
PC11	0.271	2.255	99.217
PC12	0.094	0.783	100.000

*Eigenvalues greater than one indicate PCs explaining the dataset variance.

The scree plot explained the variance in the pyrethrum plant as visualized in Figure 8. The first principal component (PC1) accounted for 26.67% of the total variance and exhibited high positive loadings for mature stalk height (*MSH*), internode length (*SIL*), floral head diameter (*FHD*), and peduncle length (*FPL*). These traits are closely associated with plant size, architecture, and structural biomass, indicating that PC1 primarily captures variations in plant growth form and above-ground biomass. The strength and significance of these traits on PC1 also suggest a high correlation, implying potential redundancy that can be exploited. The strong loadings for stalk height, internode length, and peduncle length in PC1 underscore the importance of plant architecture as a critical determinant of harvester geometry. These traits directly influence the required gathering width, finger or blade clearance, and cutting height adjustments of the harvesting unit. In practical terms, taller plants with longer internodes necessitate adjustable reel or cutter-bar positioning to minimize unharvested biomass and reduce cutting losses. PC2 explained 14.11% of the variance and was characterized by strong loadings for the coefficient of static friction (μ_s), cutting force (*CF*), and picking force (*PF*). These traits reflect the resistance encountered during mechanical manipulation and harvest, highlighting PC2 as an axis of harvestability and material handling variation. Identifying this component is particularly valuable for designing and selecting floral varieties optimized for mechanical harvesting, where lower cutting and picking forces are desirable. The contribution of cutting force, plucking force, and friction coefficients in PC2 reflect their strength in the forces encountered during detachment and conveyance. These parameters inform the selection of blade sharpness, motor torque, speed, and conveyor material, ensuring the harvester can overcome resistance without damaging flowers or consuming excessive energy. The third principal component (PC3), contributing 10.71% to the total variance, also featured a prominent loading for the coefficient of friction and for a variable associated with floral canopy weight (*FCW*). This suggests an axis combining frictional and mass-related properties, possibly relevant in scenarios where material movement or mechanical sorting is involved. Traits such as *CF* and *PF* showed moderate negative contributions to this component, suggesting inverse relationships that warrant further investigation in the context of mechanical processing. PC4 accounted for 10.27% of the variance and had its highest loading from repose angle (θ), which indicates flowability and material stability when heaped. Alongside a moderate loading from peduncle diameter (*FPD*), this component reflects variations in bulk material behaviour and pile stability. Such traits

are essential in the design of post-harvest handling and storage systems, where physical behavior under static and dynamic conditions influences efficiency and safety. The fifth principal component (PC5), which explained 9.21% of the variance, was dominated by moisture content (*MC*) and included contributions from repose angle. This axis likely represents moisture-dependent physical behavior, such as compressibility and storage dynamics. High moisture levels influence floral compressibility, degradation rates, and the suitability of biomass for long-term storage or processing, making this component especially relevant to post-harvest engineering and preservation, such as the design of drying units and temporary storage systems integrated into the harvester.

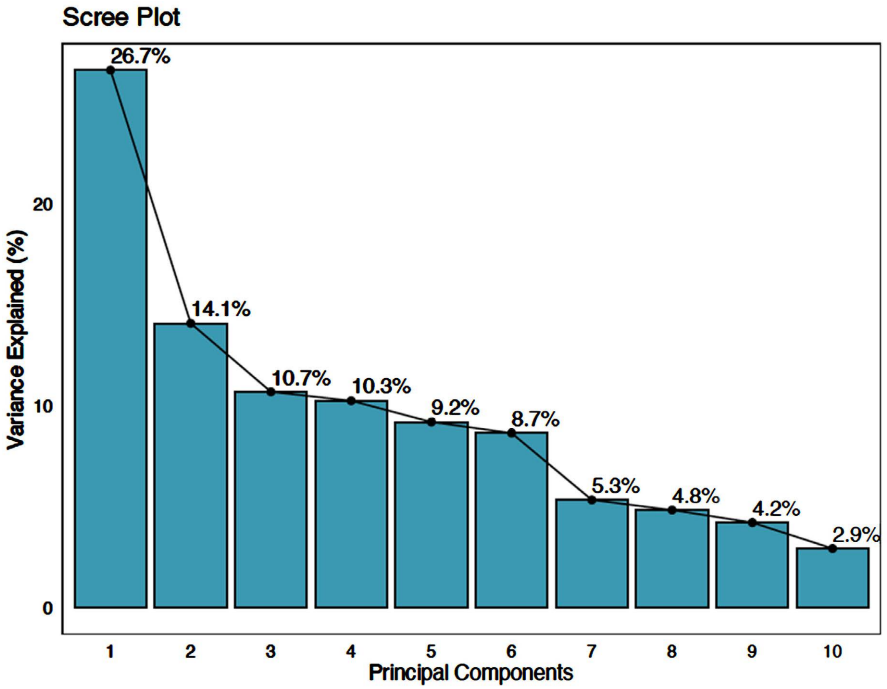

Figure 8. Scree plot of principal components explaining variance of pyrethrum traits.

Further analysis revealed different contributions of variables in PC1 and PC2, as shown in Figure 9 alongside Table 2. Mature stalk height and internode length were well-represented in PC1, whereas the coefficient of friction showed high representation in both PC2 and PC3. Repose angle and moisture content had strong representations in PC4 and PC5, respectively. These findings confirmed the dominant influence of certain traits on specific components. At the same time, they validated the interpretation of the components to reinforce the importance of these traits in determining the physical and mechanical behaviour of floral biomass for the design of precision harvesters.

Qualitative representation into the principal components revealed varying degrees of qualitative contributions of variables into PC1 and PC2, as shown in Figure 10. The arrow's length shows the representation quality. In contrast, the colour shows the contribution of the variables along PC1 and PC2.

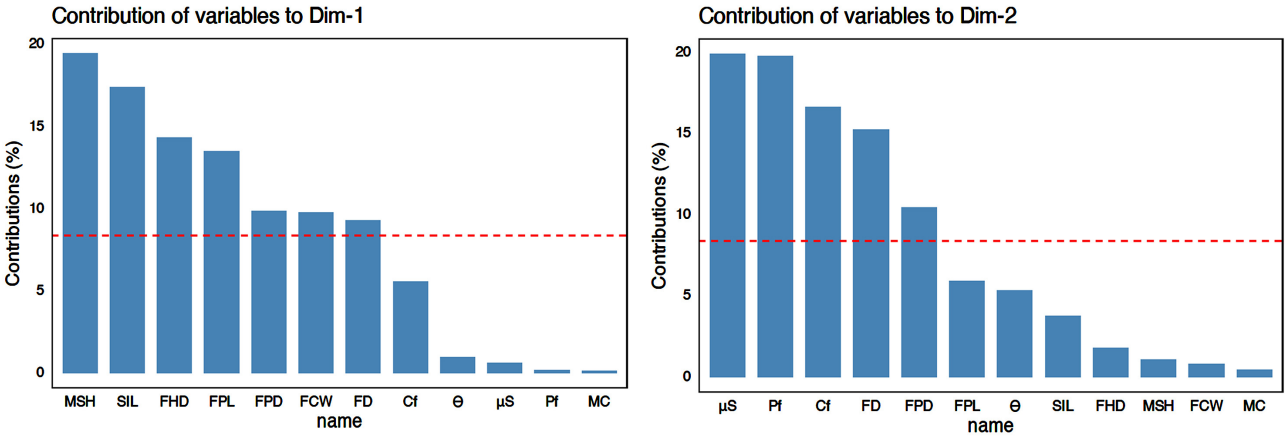

Figure 9. Variable contribution to principal components.

Table 2. Variable contributions to principal components (%).

Variable	Dim.1	Dim.2	Dim.3	Dim.4	Dim.5
MSH	19.368	0.984	2.245	3.745	6.801
FPL	13.420	5.834	6.417	0.103	5.247
FD	9.207	15.150	0.050	4.683	1.751
FHD	14.244	1.711	5.550	0.475	10.970
FPD	9.789	10.331	0.024	8.181	0.581
FCW	9.681	0.703	30.213	0.000	6.237
SIL	17.294	3.650	2.847	4.156	0.045
μs	0.513	19.811	36.933	3.232	2.323
CF	5.461	16.546	5.414	7.685	0.237
PF	0.088	19.686	6.199	4.575	1.268
MC	0.045	0.366	3.921	13.931	53.822
θ	0.891	5.229	0.188	49.233	10.717

Qualitative contributions of all variables revealed variations in qualitative contribution ($\cos^2$) to principal components. The PCA effectively categorized complex interrelationships among morpho-physical and mechanical properties of floral biomass into five principal components (Table 3). These components highlight key plant trait groupings relevant to mechanization and post-harvest handling. PC1 captures size and architectural traits, PC2 and PC3 represent mechanical resistance and frictional properties, while PC4 and PC5 encompass flowability and moisture-related behaviour. The insights from this analysis guided the trait prioritization in developing precision harvest and processing equipment and enhancing post-harvest management strategies for floral pyrethrum biomass. Table 3 presents the quality of representation of each variable across the first five principal components (PCs) derived from Principal Component Analysis (PCA), as measured by squared cosine ($\cos^2$) values. These values indicate how well the var-

iance of each original variable is captured by a given component, with higher values signifying more substantial alignment. Notably, the first principal component (Dim.1) accounts for considerable variation in morphological traits such as mature stalk height (*MSH*; 0.620), flower peduncle length (*FPL*; 0.429), flower head diameter (*FHD*; 0.456), and stalk internode length (*SIL*; 0.553), suggesting that Dim.1 predominantly captures structural plant characteristics. In contrast, traits such as flower canopy width (*FCW*), mean static coefficient of friction (μ_s), cutting force (*CF*), and plucking force (*PF*) show stronger associations with Dim 2 and Dim 3, indicating that these components encode mechanical and compositional properties rather than size.

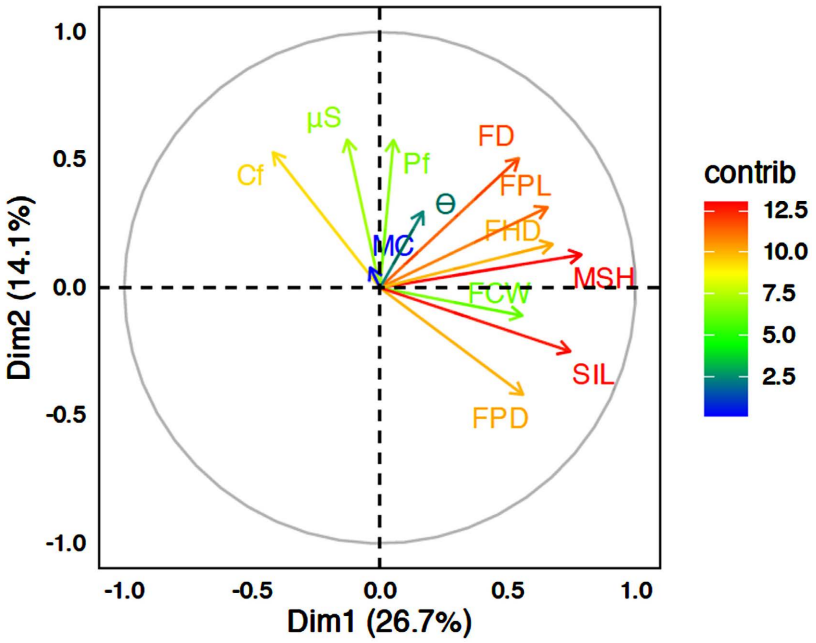

Figure 10. Contribution of variables in the first and second dimensions of PCs.

Moisture content (*MC*) and repose angle (θ) exhibit minimal representation in the leading components but dominate in Dim 5 (0.595) and Dim 4 (0.606), respectively. This observation suggests that while these traits are integral to understanding cutting dynamics, they encapsulate unique variance orthogonal to that captured by earlier PCs. The divergence in representation highlights the multidimensionality of the underlying trait space and affirms the need to retain later components to preserve explanatory power for these specialized variables. Consequently, the PCA structure underscores precise partitioning between morphological, mechanical, and cutting-related dimensions, providing a robust foundation for trait-informed modelling and optimization in crop mechanization systems.

The individual PCA plot, **Figure 11**, complements this trait decomposition by illustrating how each simulated observation projects onto the principal component space defined by the dominant trait dimensions. In the biplot of PC1 versus PC2, individuals are dispersed along gradients primarily defined by structural

traits such as mature stalk height and flower head diameter, with precise spatial separation that reflects underlying morphological variability. Meanwhile, individuals positioned along PC2 exhibited variability driven more by frictional and mechanical traits, including cutting and plucking forces. This spatial organization offers critical insight into how simulated plant architectures cluster in trait space, validating the biological realism of the process and providing a visual anchor for linking individual plant configurations to specific optimization objectives, particularly those targeting efficient machine-crop interaction.

Table 3. Quality of representation of pyrethrum variables ($\cos^2$) into the dimensions of PCs.

Variable	Dim.1	Dim.2	Dim.3	Dim.4	Dim.5
MSH	0.620	0.017	0.029	0.046	0.075
FPL	0.429	0.099	0.082	0.001	0.058
FD	0.295	0.256	0.001	0.058	0.019
FHD	0.456	0.029	0.071	0.006	0.121
FPD	0.313	0.175	0.000	0.101	0.006
FCW	0.310	0.012	0.388	0.000	0.069
SIL	0.553	0.062	0.037	0.051	0.000
μs	0.016	0.335	0.475	0.040	0.026
CF	0.175	0.280	0.070	0.095	0.003
PF	0.003	0.333	0.080	0.056	0.014
MC	0.001	0.006	0.050	0.172	0.595
θ	0.028	0.089	0.002	0.606	0.118

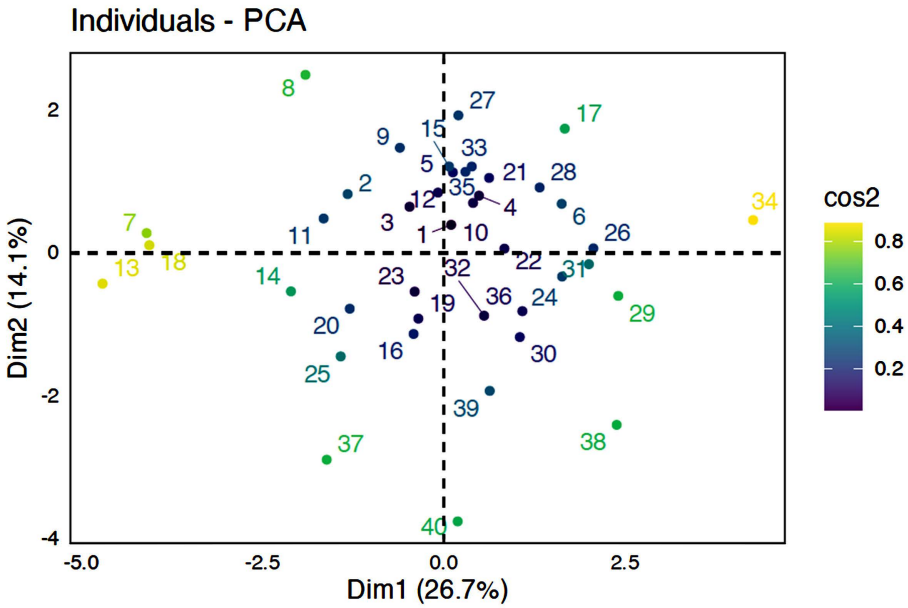

Figure 11. Individual plot of the data points.

3.4. Surface Response Models

Response Surface Methodology (RSM) was selected to model and optimize the nonlinear relationships between critical harvesting forces and plant characteristics. RSM has proven effective in predicting and optimizing biological and engineering processes where multiple interdependent variables influence mechanical performance [55]. For instance, the second-order surface response model explains well the bending, shearing, and compressive forces that occurred during mechanical picking of pyrethrum flowers, as shown in **Figure 12**. The second-order regression model revealed the relationship between picking force, cutting force, and mechanical compressibility and offered a deeper understanding of the complex mechanical interactions occurring during flower detachment. While the first-order models failed to capture meaningful relationships, evidenced by low R^2 (0.03) and non-significant predictors, the second-order model reveals a more nuanced curvilinear relationship (Equation (23)). Such rheolo-mechanical curvilinearities aligned well with the known nonlinear behaviour of biological tissues under mechanical forces during harvesting [23] [56] [57]. The surface response model is shown in Equation (23) as a second-order quadratic.

$$z = \beta_0 + \beta_1 x + \beta_2 y + \beta_3 xy + \beta_4 x^2 + \beta_5 y^2 + \varepsilon \tag{23}$$

where ε accounts for the random error in the model and Equation (23) can be expressed in Equation (24),

$$\text{Plucking force } (\text{PF}) = 4.2664 - 3.8308 * CF + 0.90098 * \acute{c} + 234.23 * CF * \acute{c} - 21.824 * CF - 3301 * \acute{c} + \varepsilon \tag{24}$$

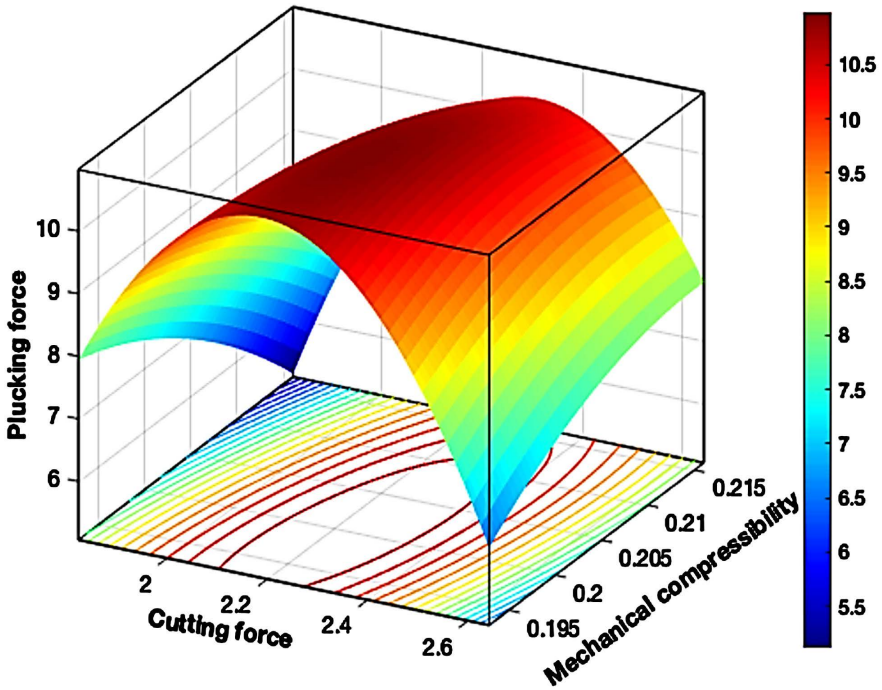

Figure 12. Surface response of plucking, cutting, and mechanical compressibility forces of pyrethrum flowers.

The quadratic term for cutting force (x^2) is statistically significant (p = 0.0006), suggesting that the relationship between cutting force and picking force is not simply additive but shaped by increasing or diminishing returns at higher force levels. This observation is particularly relevant in biomechanical studies of plant material, where force-displacement relationships rarely follow a straight line. For instance, [58] emphasized that biological materials such as stems, leaves, and flowers exhibit nonlinear responses due to viscoelasticity, cellular structure, and moisture content. This significant quadratic term likely reflects the existing complexity, possibly indicating that beyond a certain cutting force threshold, increases no longer translate proportionally to picking force due to tissue rupture or fibre alignment. On the other hand, neither the linear nor the quadratic terms for mechanical compressibility were statistically significant. However, their inclusion in the model improved the overall explanatory power (R^2 = 0.38) compared to the linear model (R^2 = 0.03), as shown in Table 4. These findings suggest that while compressibility alone may not predict picking force effectively, its interaction with cutting force (though non-significant at p = 0.43) contributes to a more robust model fit. In practical terms, this reinforces the idea that picking force cannot be understood as a function of cutting force or compressibility in isolation, but rather as a dynamic outcome of how these mechanical properties interact. This dynamic interplay is consistent with the literature in postharvest and agricultural engineering. According to [59], separation forces during harvesting often depend on the combined cutting resistance, compressive deformation, and tissue cohesion, which vary significantly with floral morphology and maturity. Thus, a second-order model is well-suited to capture the bending, shearing, and compressive forces that co-occur during mechanical picking. This model provides an engineering basis for selecting appropriate blade torque and plucking unit force while accounting for compressibility effects on the onboard temporal storage systems. This ensures efficient flower detachment without excessive tissue damage or unnecessary energy use.

Table 4. Cutting force model coefficients and performance metrics.

Model coefficients					Performance metrics						
	Intercept	SE	t.Stat	p-value	n	DoF	RMSE	R^2	R^2 adj.	F. Stat	p-value
β_0	−125.38	496.31	−0.25263	0.80207	40	37	1.85	0.38	0.288	4.16	0.00467
β_1	50.309	71.986	0.69887	0.48939							
β_2	801.39	4332	0.18499	0.85433							
β_3	234.23	296.26	0.79061	0.43465							
β_4	−21.824	5.7997	−3.7629	0.00063539							
β_5	−3301	9583.2	−0.34446	0.73263							

3.5. Surface Response Models of Bulk Volumetric Coefficients

Figure 13 shows the relationship between dry floral volume, volumetric expan-

sion coefficient, and dry unit flower volume. The models revealed an incongruent relationship between the volumetric expansion coefficient and dry flower volume. Such an effect revealed that flowers with higher expansion potential during hydration can undergo more shrinkage upon drying, resulting in smaller final volumes. These findings align with tissue mechanics and shrinkage kinetics and behaviour in floral structures during dehydration and desiccation [60] [61]. Further, the positive correlation of unit floral volume to volumetric expansion coefficients aligns with bulk biological materials theories, where larger floral structures retain more absolute mass and structural integrity after drying, yielding higher final volumes [62] [63].

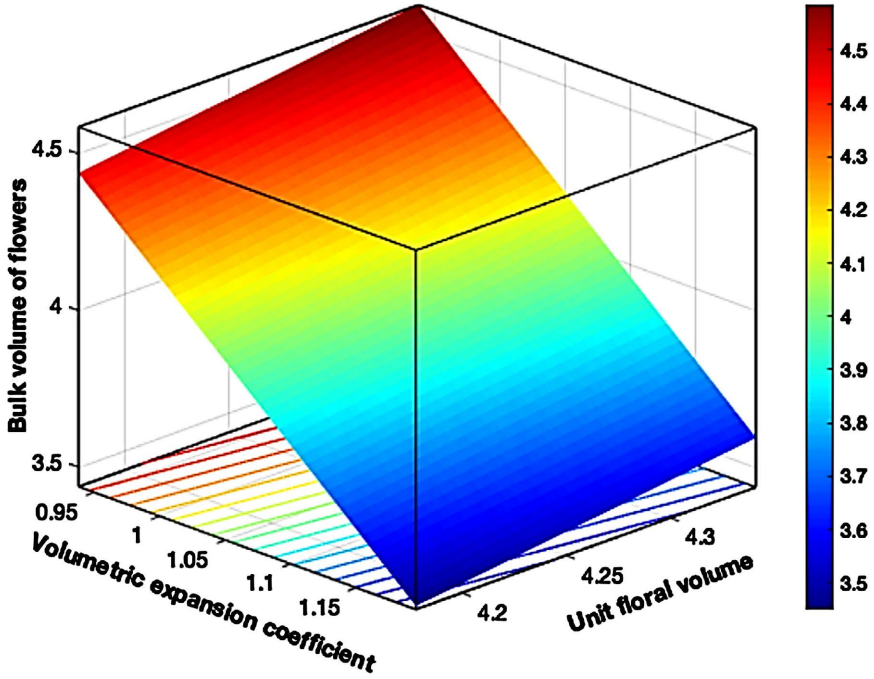

Figure 13. Surface response of volumetric handling coefficients.

The first-order regression model evaluating the volume of dry flowers (z) as a function of the volumetric expansion coefficient (x) and unit floral volume (y) is shown in Equation 25. The coefficients and performance metrics of the model are shown in **Table 5.** The models demonstrated a statistically robust and highly predictive relationship. Both independent variables are highly and significantly associated ($p < 0.001$) with the dependent variable, where x ($p = 2.93e{-}41$) and y ($p = 2.28e{-}14$) showed a strong negative and positive relationship, respectively. The model accounted for 99.3% of the volume of dry flowers ($R^2 = 0.993$), with a very low root mean squared error (RMSE = 0.0183), suggesting a near-perfect linear fit. This observation indicates that the model performs exceptionally well in capturing the variations in floral drying outcomes during handling. Further, the strong predictive fit informs the design of hopper capacity and compression units, ensuring smooth handling of floral biomass during harvesting and transport.

$$z = \beta_0 + \beta_1 x + \beta_2 y + \varepsilon \tag{25}$$

Table 5. Bulk volume pyrethrum handling model coefficients and performance metrics.

Model coefficients					Performance metrics					
Intercept	SE	t. stat	p-value	n	DoF	RMSE	R^2	R^2 adj.	F. Stat	p-value
(β_0) 4.2664	0.3089	13.813	3.531e−16	40	37	0.0183	0.993	0.993	2.58e+03	1.81e−40
x (β_1) −3.8308	0.0536	0.0536	2.928e−41							
y (β_2) 0.90098	0.0748	12.046	2.276e−14							

3.6. Cutting Force vs Moisture Content and Mature Stalk Height

Figure 14 shows the variation of cutting force (*CF*), with mature stalk height (*MSH*) and moisture content (*MC*) of mature pyrethrum stalks. The surface response regression revealed a first-order linear model expressed using Equation (26).

$$z = \beta_0 + \beta_1 x + \beta_2 y + \varepsilon \tag{26}$$

where ε accounts for the random error in the model and Equation (26) can be rewritten into Equation (27).

$$\text{Cutting force } (CF) = -0.023323 + (0.044707 * MC) - (0.0015509 * MSH) + \varepsilon \tag{27}$$

where z denotes the dependent variable (cutting force), and x and y represent the independent variables, specifically *MC* and *MSH*, respectively.

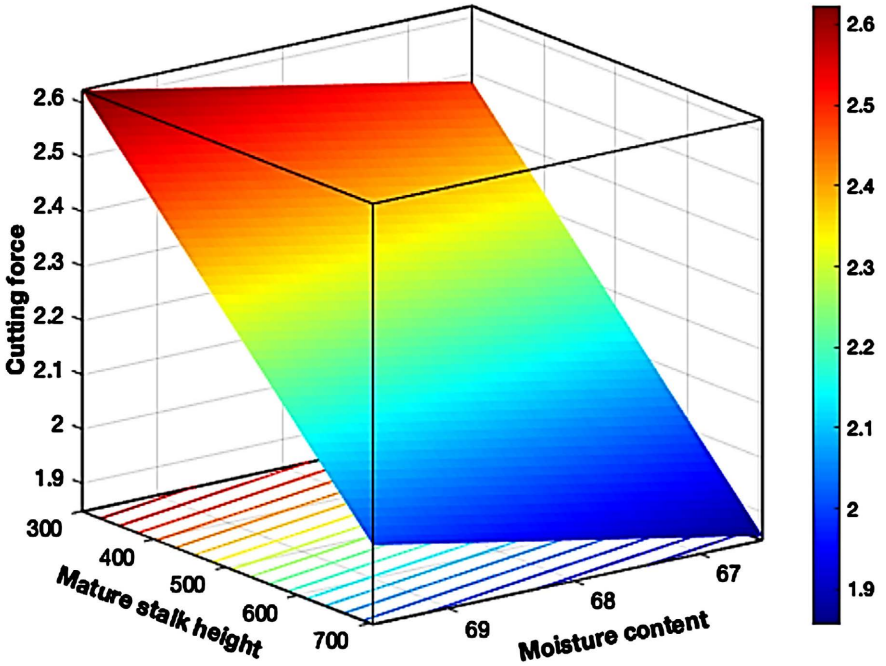

Figure 14. Response surface of cutting force, mature stalk height, and moisture content of pyrethrum.

The coefficients and performance metrics of the model are shown in Table 6. The model fitted 40 data points, with 37 degrees of freedom remaining for the error term,

indicating the subtraction of three parameters (intercept, *x*, and *y*) from the total sample size. The root mean squared error (RMSE) is approximately 0.229, reflecting the residuals' average magnitude. The coefficient of determination, $R^2 = 0.226$, suggests that about 22.6% of the variation in the dependent variable z can be explained by the linear effects of *x* and *y*. The adjusted R^2, which penalizes the inclusion of additional predictors, is slightly lower at 0.184, highlighting modest explanatory power. The F-statistic for the model is 5.41, with an associated p-value of 0.00868. The p-value is less than 0.05, and the response surface model is statistically significant, performing better than a constant-only model, implying that at least one of the predictors contributes meaningfully to explaining the z factor.

Individual regression coefficients indicated that the intercept (β_0) is estimated at −0.0233 with a standard error of 3.1323 and a t-statistic of −0.0074, leading to a p-value of 0.9941. The result is not statistically significant and indicates that whenever both *x* and *y* are zero, the predicted mean of *z* is essentially zero. However, the reliability of this estimate is extremely low. The *x* (β_1) coefficient is 0.0447 with a standard error of 0.0465, and the resultant t-statistic is 0.9605 while the p-value is 0.3430, suggesting that x is not a statistically significant predictor of *z* at the 5% level. In contrast, the y coefficient (β_2) is −0.00155 with a standard error of 0.000475, and the corresponding t-statistic is −3.2653 while the p-value is 0.00236, which is statistically significant at the 1% level. These findings indicate a strong negative association between *MSH* and cutting force, implying that for every unit increase in *MSH*, there was an expected decrease of approximately 0.00155 units in cutting force, holding *MC* constant. A similar effect was reported in literature [64].

The regression model is statistically significant overall, as evidenced by the F-test (p = 0.00868), affirming that it explains a non-negligible proportion of the variability in the cutting force compared to a model with no predictors. Only *y* (*MSH*) exhibits a statistically significant influence on *z* (cutting force), demonstrating a meaningful negative linear relationship among the individual predictors. Neither *x* (*MC*) nor the intercept contributed significantly within this linear framework. Nevertheless, the relatively low R^2 (22.6%) implies that the model accounts for a limited share of the total variability in *z*, indicating that additional variables or nonlinear terms may be necessary to improve the predictive performance of the surface response model. Therefore, this model can guide blade height adjustment and energy input in connection with crop moisture status, ensuring efficient cutting while minimizing excessive power demand.

Table 6. Response surface model coefficients of *MSH*, Moisture content, and cutting force.

Model coefficients					Performance metrics					
Intercept	SE	t. stat	p-value	*n*	DoF	RMSE	R^2	R^2 adj.	F. Stat	p-value
(β_0) −0.0233	3.1323	−0.0074	0.9941	40	37	0.229	0.226	0.184	5.41	0.00868
x (β_1) 0.0447	0.0465	0.9605	0.3430							
y (β_2) −0.00155	0.00047	−3.2653	0.00236							

3.7. Surface Response Model of Mature Stalk Height, Flower Canopy Width and Stalk Internode Length

The surface response model of mature stalk height (*MSH*), flower canopy width (*FCW*) and stalk internode length (*SIL*) is shown in Figure 15 alongside the model coefficient in Table 7**.** The surface response revealed important plant structural and morpho-physical development patterns for designing precision harvesting machinery. Although *FCW* did not significantly predict stalk height in the current model, its biological role should not be dismissed. Plant architecture studies have shown that canopy structure can affect light interception, influencing photosynthetic capacity and growth efficiency, and thus the *MSH*, biomass accumulation, and overall plant height over time [65]. Therefore, while the immediate statistical contribution of *FCW* to stalk height may appear limited, its indirect physiological impact may be more pronounced under different environmental or genetic contexts. Thus, the surface response model supports a strong association between internode length and mature stalk height and is consistent with literature across multiple plant species. The role of *FCW* on *MSH*, although not very significant compared to internode length, as shown in Figure 15, its indirect role in precision harvesting remains plausible.

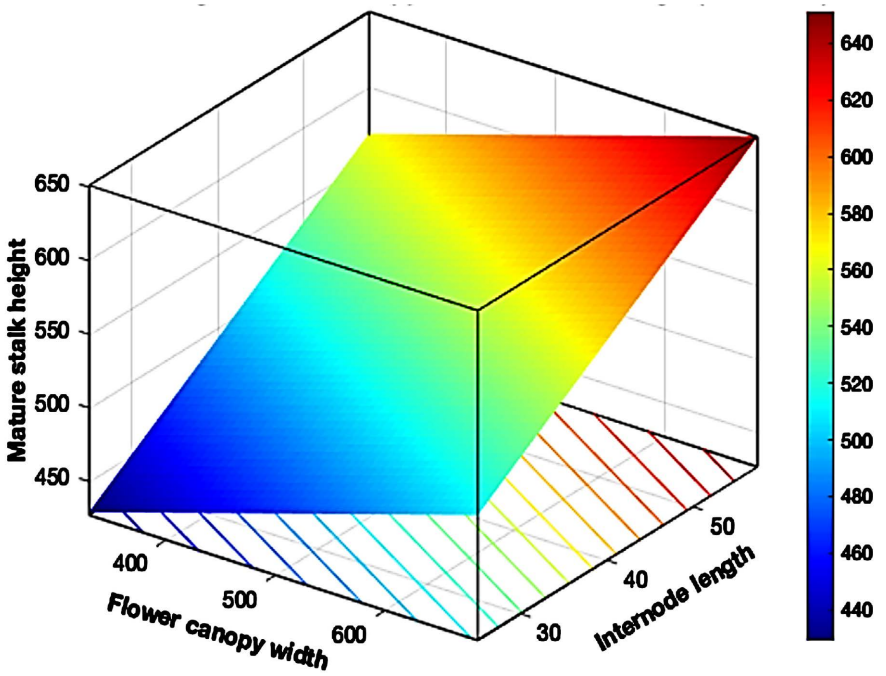

Figure 15. Surface response model of *MSH*, *FCW*, and *SIL* of pyrethrum.

The surface response model coefficient and performance (Table 7) indicated that internode length is a statistically significant predictor for mature stalk height ($p = 0.0147$). In contrast, flower canopy width shows a positive but statistically non-significant relationship ($p = 0.1015$). The coefficient estimates further elucidate the nature of the relationships. The intercept, estimated at approximately

244.93, is highly significant (p = 0.0035), indicating this study's baseline value of *MSH*. These findings align with studies that emphasized the role of internodal elongation in overall plant height in precision handling during harvest. For instance, in [66] and [67], variations in internode length and elongation patterns of bamboo species and maize, respectively, affected mature plant height and yield in foxtail millet [68]. These findings indicate internode characteristics are central to stalk elongation and overall plant height in diverse plant taxa and affect precision harvesting. The surface response coefficient of determination (R^2) is 0.278, indicating that approximately 27.8% of the variability in mature stalk height is explained by *FCW* and *SIL*. The adjusted R^2, which accounts for the number of predictors, is slightly lower at 0.238, reflecting a minor penalty for inclusion of variables relative to the number of observations. The root mean squared error (RMSE) is 68.6, which measures average prediction error in the same units as the response variable. Thus, the model supports a strong association between internode length and mature stalk height, and is consistent with literature across multiple plant species, and can be considered an essential aspect in the design of precision harvesters. This relationship informs the design of gathering units and cutter-bar clearance, indicating that internode length should be prioritized when setting stalk entry dimensions. The response surface model is expressed as (Equation (28)), and the parameters are indicated in **Table 7**.

$$z = \beta_0 + \beta_1 x + \beta_2 y + \varepsilon \tag{28}$$

Table 7. Surface response model of *MSH*, *FCW*, and *SIL* of pyrethrum.

Model coefficients					Performance metrics						
	Intercept	SE	t.stat	p-value	n	DoF	RMSE	R^2	R^2 adj.	F. Stat	p-value
(β_0)	244.93	78.468	3.1214	.0034843	40	37	68.6	0.278	0.238	7.11	0.00244
x (β_1)	0.23401	0.13934	1.6794	0.10151							
y (β_2)	4.2784	1.672	2.5589	0.014725							

3.8. Surface Response of Cutting Force, Moisture Content vs Picking Force

Figure 16 shows the surface response surface model of cutting force (*CF*) vs moisture content (*MC*) and picking force (*FP*) of pyrethrum. A downward curvilinearly open parabola characterized the relationship, and the optimal response model was quadratic and can be expressed using Equation (29).

$$z = \beta_0 + \beta_1 x + \beta_2 y + \beta_3 xy + \beta_4 x2 + \beta_5 y2 + \varepsilon \tag{29}$$

Table 8 indicates that the model exhibits strong explanatory capacity, with an R^2 of 0.892 and an adjusted R^2 of 0.876, indicating that the model accounts for nearly 89.2% of the variability in the response. The overall model fit is statistically significant, as confirmed by an F-statistic of 56.3 and a p-value of 1.79×10^{-15}. Additionally, the RMSE of 0.0894 demonstrates high precision in the model's resid-

ual estimates. Inspection of the individual regression coefficients reveals that most predictors, including the linear terms x and y, the interaction term x^*y, and the quadratic term x^2, are not statistically significant at the 5% level. The only exception is the quadratic term for y (y^2), which is highly significant ($p \approx 1.14 \times 10^{-17}$) and has a negative coefficient. Further, the quadratic relationship provides a basis for calibrating blade speed and plucking force mechanisms under varying moisture regimes, preventing flower damage while maintaining detachment efficiency.

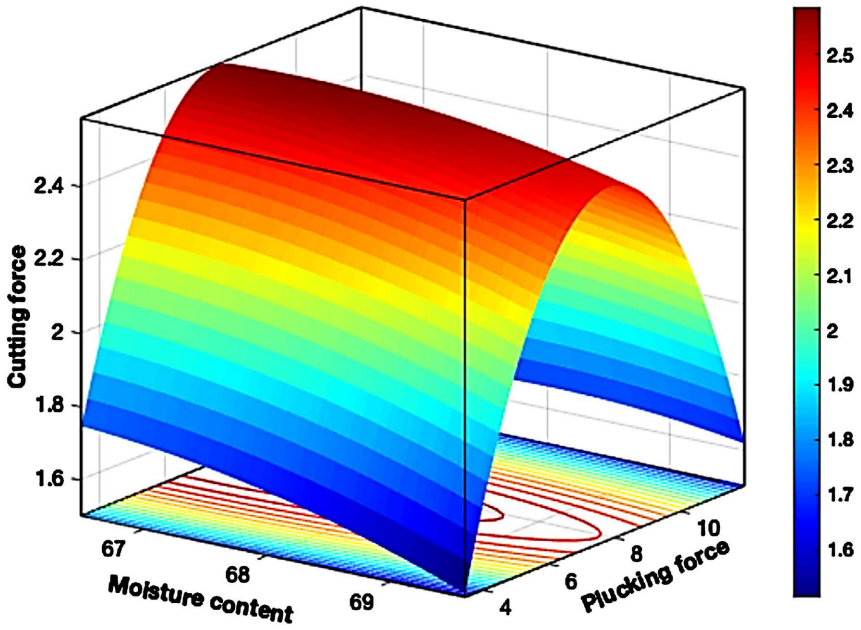

Figure 16. Surface response model of cutting, plucking forces, and moisture content of pyrethrum flowers.

Table 8. Surface response coefficients of cutting Force, moisture content, and plucking force of pyrethrum.

Model coefficients					Performance metrics						
Intercept		SE	t.stat	p-value	n	DoF	RMSE	R^2	R^2 adj.	F. Stat	p-value
(β_0)	−72.4	105.86	−0.68395	0.49864	40	34	0.0894	0.892	0.876	56.3	1.79e−15
x (β_1)	2.2228	3.0871	0.72002	0.47644							
y (β_2)	0.16465	0.53506	0.30772	0.76017							
x^*y	0.0088	0.0078427	1.1229	0.26936							
x^2	−0.0171	0.022511	−0.76007	0.45245							
y^2	−0.04964	0.0030381	−16.338	1.1448e−17							

3.9. Shear Strength, Moisture Content, and Floral Diameter

Figure 17 shows an asymmetric curvilinear response surface of shear strength (τ), moisture content (MC), and floral diameter (FD). The MC increased from approximately 66.5% to 69.5%, with a notable decline in τ, reaching a minimum

approx. 68.8%, after which the τ slightly rises curvilinearly. This trend indicates a quadratic relationship between moisture content and shear strength, where intermediate moisture levels correspond to reduced shear strength. Studies of other biological materials by [69] described a similar effect. The non-linearity between shear strength, moisture content, and *FD* reflects how variations in internal water content can alter the mechanical integrity of the plant materials. As the flower diameter increases from 28 mm to approximately 40 mm, shear strength increases. The shape of the response surface also indicates that this effect is not uniform across all moisture levels, highlighting the significance of the interaction between the two variables.

The interaction between *MC* and *FD* is particularly evident in the twisting of the response surface and the non-parallel contour lines at the base. This observation indicates that the effect of one variable on shear strength depends on the other variable's level. Evidently, the lowest τ values are observed at high *MC* at the lowest *FDs*, underscoring the synergistic nature of these factors in the design of precision harvesting components. Previous studies evaluated other biological plant materials' hardness, breaking force, and τ and reported similar observations in response to *MC* [69] [70]. This model can be applied to optimize blade edge sharpness and cutting angle, ensuring that the harvester's cutting unit matches τ thresholds across all flower sizes and moisture levels.

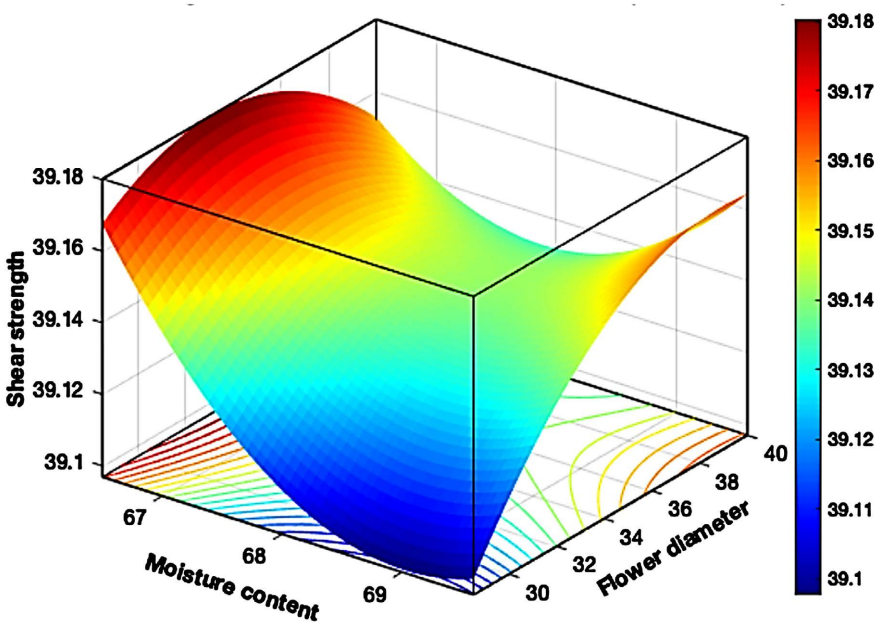

Figure 17. Response surface model of shear strength, moisture content, and pyrethrum floral diameter.

4. Conclusions and Future Research Works

4.1. Conclusions

The following conclusions were drawn from this study.

- Mature stalk height of pyrethrum increases with floral canopy width and in-

ternode length.

- Cutting force followed a linearly increasing trend with reduced stalk height and moisture content.
- Cutting and picking forces are quadratically correlated with pyrethrum's mechanical compressibility and moisture content.
- The correlation between shear strength, moisture content, and floral diameters of pyrethrum is curvilinearly quadratic.
- The lowest shear strength of pyrethrum occurred at high moisture contents at the lowest floral diameters.
- Second-order quadratic curvilinear surface response models characterize and effectively optimize pyrethrum mechanical parameters to design precision harvesting components.
- All bio-physical-mechanical characteristics of pyrethrum were highly significant ($p < 0.01$), underscoring their critical role in the design of precision harvesting components.
- The study provides a foundational insight for designing mechanized precision harvesters to reduce drudgery and health hazards associated with laborious handpicking.

4.2. Future Research Works

Future studies need to focus on the varietal differences and genetic variations among pyrethrum and their influence on morphological and physio-mechanical properties that would affect the applicability of the developed models. Unlike static laboratory and field measurements, dynamic machine-crop interactions under real harvesting conditions can introduce additional complexities over and above morphological variabilities. As such, further work should prototype harvester trials and validate these findings across different environments to enhance the generalized utilization of the results.

Author Contributions

A. M. and **F. M.**: Research conceptualization, Methodology, Field investigations, Machinery preparation, Experimental design, Data collection, Data curation, Data Analysis, Interpretation, Software, Formal analysis, Modeling, Validation, Database, Writing the original manuscript, Comprehensive revision, and Final editing and manuscript structure. **S. M.**: Research administration, Resources, Supervision, and Research mentorship.

Acknowledgement and Funding

This research received operational support from the Kenya Education Network Trust (KENET), the National Research and Education Network (NREN) of Kenya, KENET/ENG/2025/1.

Data Availability Statement

Datasets utilized in this study can be made available by the corresponding author

on reasonable request.

Permission for Land Studies

The authors declare that all the field sampling and machinery investigations on land observed local rules and regulations.

Conflicts of Interest

Authors declare no known competing relationships or conflicting financial interests.

References

[1] Biošić, M., Varga, F., Dabić, D., Topalović, I., Šatović, Z. and Grdiša, M. (2020) Matrix Solid-Phase Dispersion Optimization for Determination of Pyrethrin Content in Dalmatian Pyrethrum (*Tanacetum cinerariifolium*/Trevir./Sch. Bip.) by Liquid Chromatography. *Industrial Crops and Products*, **145**, Article 111999. https://doi.org/10.1016/j.indcrop.2019.111999

[2] Verma, P.P.S., Kumar, D., Kumar, B., Padalia, R.C. and Kumar, A. (2023) Flower Yield Potential of Pyrethrum (*Chrysanthemum cinerariaefolium* L.) under Various NPK Levels in the Lower Hills of Uttarakhand, India. *Journal of Agricultural Sciences-Sri Lanka*, **18**, 432-442. https://doi.org/10.4038/jas.v18i3.9811

[3] Suraweera, D.D., Groom, T., Taylor, P.W.J., Jayasinghe, C.S. and Nicolas, M.E. (2017) Dynamics of Flower, Achene and Trichome Development Governs the Accumulation of Pyrethrins in Pyrethrum (*Tanacetum cinerariifolium*) under Irrigated and Dryland Conditions. *Industrial Crops and Products*, **109**, 123-133. https://doi.org/10.1016/j.indcrop.2017.07.042

[4] Dongdong, D. and Jun, W. (2016) Research on Mechanics Properties of Crop Stalks: A Review. *International Journal of Agricultural and Biological Engineering*, **9**, Article 6.

[5] Nag, R.H., Sharma, P.K., Kushwaha, H.L., B.S., M., Rathod, S.K., Kumar, A.K., *et al.* (2024) Assessing Physical Characteristics for Precision Harvester Design: A Comparative Study of Spinach, Fenugreek, and Coriander Leafy Vegetables. *Journal of Scientific Research and Reports*, **30**, 631-639. https://doi.org/10.9734/jsrr/2024/v30i92391

[6] Heidari, A. and Chegini, G.R. (2011) Determining the Shear Strength and Picking Force of Rose Flower. https://openurl.ebsco.com/contentitem/gcd:89479176?sid=ebsco:plink:crawler&id=ebsco:gcd:89479176

[7] Kumar, M., Sahoo, P.K., Kushwaha, D.K., Mani, I., Pradhan, N.C., Patel, A., *et al.* (2024) Force and Power Requirement for Development of Cumin Harvester: A Dynamic Approach. *Scientific Reports*, **14**, Article No. 13666. https://doi.org/10.1038/s41598-024-64473-y

[8] Eliçin, A.K., Sessiz, A. and Pekitkan, F.G. (2019) Effect of Various Knife Type, Cutting Angle and Speed on Cutting Force and Energy of Grape Cane. *European Journal of Science and Technology*, **15**, 519-525. https://doi.org/10.31590/ejosat.532914

[9] Lu, W., Li, X., Zhang, G., Tang, J., Ni, S., Zhao, C., *et al.* (2023) Tensile and Shear Mechanical Properties of Laver (*Porphyra yezoensis* Ueda). *International Journal of Food Properties*, **26**, 1005-1019. https://doi.org/10.1080/10942912.2023.2197567

[10] Wang, Y., Li, D., Nie, C., Gong, P., Yang, J., Hu, Z., *et al.* (2023) Research Progress on the Wear Resistance of Key Components in Agricultural Machinery. *Materials*,

16, Article 7646. https://doi.org/10.3390/ma16247646

[11] T N, A., Sahoo, P.K., Kushwaha, D.K., Pradhan, N.C., Kumar, K., V, S.K., *et al.* (2025) Static and Dynamic Cutting Forces in Coriander Crop Harvesting: Engineering Insights for Harvester Optimization. *Smart Agricultural Technology*, **10**, Article 100772. https://doi.org/10.1016/j.atech.2025.100772

[12] Toleu, Z. and Liu, J. (2024) Dynamic Cutting Properties of Miscanthus (Giganteus) Stems Using an Impact Tester. *Agri Engineering*, **6**, 1987-2000. https://doi.org/10.3390/agriengineering6030116

[13] Kumawat, L. and Raheman, H. (2023) Determination of Engineering Properties of Onion Crop Required for Designing an Onion Harvester. *Cogent Engineering*, **10**, Article 2191404. https://doi.org/10.1080/23311916.2023.2191404

[14] Nurhasanah, A., Hermawan, W., Mandang, T., Unadi, A., Budiharti, U., *et al.* (2023) Engineering Properties of Sorghum Bioguma-Variety for Designing Appropriate Thresher and Chopper Machine. *AIMS Agriculture and Food*, **8**, 720-735. https://doi.org/10.3934/agrfood.2023039

[15] Kumar, S., Mahapatra, M., Behera, D., Pradhan, P.L., Swain, S.K., Rath, I., *et al.* (2023) Effect of Stem Diameter, Cutting Speed and Moisture Content on Cutting Torque for Green Gram Harvesting. *International Journal of Bio-Resource and Stress Management*, **14**, 1127-1132. https://doi.org/10.23910/1.2023.3593b

[16] Ali, K.A.M., Huang, X., Zong, W. and Abdeen, M.A.M. (2020) Mechanical Structure and Operating Parameters of Sunflower Harvesting Machines: A Review. *International Agricultural Engineering Journal*, **29**, 143-153.

[17] Tavakoli, H. and Jafari, A. (2009) Some Engineering Properties of Barley Straw. *Applied Engineering in Agriculture*, **25**, 627-633.

[18] Mushtaq, S.A., Khar, S., Sharma, S. and Singh, J. (2024) Study of Morphological Characteristics of Basmati-370 Paddy Variety Pertinent to Paddy Harvester Design. *International Journal of Statistics and Applied Mathematics*, **6**, 1-3.

[19] Kumar, A., Antil, S.K., Rani, V., Antil, P., Jangra, D., Kumar, R., *et al.* (2020) Characterization on Physical, Mechanical, and Morphological Properties of Indian Wheat Crop. *Sustainability*, **12**, Article 2067. https://doi.org/10.3390/su12052067

[20] Muzamil, M., Mani, I., Kumar, A. and Lande, S. (2016) Influence of Moisture Content, Loading Rate and Internode Position on the Mechanical Properties of Paddy and Wheat Straw. *International Journal of Bio-Resource and Stress Management*, **7**, 280-285. https://doi.org/10.23910/ijbsm/2016.7.2.1469b

[21] Abd El-Gany, H.M., El-Sahhar, E.A., Mostafa, M.M. and Abd-Elhady, F.A. (2008) A Developed Machine to Harvest Carrot Crop. *Misr Journal of Agricultural Engineering*, **25**, 1163-1173. https://doi.org/10.21608/mjae.2008.152376

[22] Jahanbakhshi, A., Abbaspour-Gilandeh, Y. and Gundoshmian, T.M. (2018) Determination of Physical and Mechanical Properties of Carrot in Order to Reduce Waste during Harvesting and Post-Harvesting. *Food Science & Nutrition*, **6**, 1898-1903. https://doi.org/10.1002/fsn3.760

[23] Jin, Y., Wang, J., Chen, J., Song, Z., Zhang, R. and Zhou, R. (2024) Design and Experiment for Flexible Clamping and Conveying Device for Green Leafy Vegetable Orderly Harvester. *Agriculture*, **14**, Article 967. https://doi.org/10.3390/agriculture14060967

[24] Atallah, M. (2012) Physical and Mechanical Properties of Tomato Plant to Designa Harvest Machine. *Egyptian Journal of Agricultural Sciences*, **63**, 8-18. https://doi.org/10.21608/ejarc.2012.214361

[25] Li, Z., Lv, K., Wang, Y., Zhao, B. and Yang, Z. (2015) Multi-Scale Engineering Prop-

erties of Tomato Fruits Related to Harvesting, Simulation and Textural Evaluation. *LWT—Food Science and Technology*, **61**, 444-451. https://doi.org/10.1016/j.lwt.2014.12.018

[26] Swami, C.Y., Kumaran, G.S., Naik, R.K., Reddy, B.S. and Kumari, A.C.R. (2021) Physio-Morphological and Mechanical Propertiesof Chillies for Mechanical Harvesting. *Journal of Horticultural Sciences*, **16**, Article 2.

[27] An, X., Li, Z., Zude-Sasse, M., Tchuenbou-Magaia, F. and Yang, Y. (2020) Characterization of Textural Failure Mechanics of Strawberry Fruit. *Journal of Food Engineering*, **282**, Article 110016. https://doi.org/10.1016/j.jfoodeng.2020.110016

[28] Kaur, B., Mansi,, Dimri, S., Singh, J., Mishra, S., Chauhan, N., *et al.* (2023) Insights into the Harvesting Tools and Equipment's for Horticultural Crops: From Then to Now. *Journal of Agriculture and Food Research*, **14**, Article 100814. https://doi.org/10.1016/j.jafr.2023.100814

[29] Mulagoli, I.J.W. (2015) Revival Status of the Pyrethrum Industry in Kenya. *Acta Horticulturae*, **1073**, 27-37. https://doi.org/10.17660/actahortic.2015.1073.2

[30] Proudfoot, A.T. (2005) Poisoning Due to Pyrethrins. *Toxicological Reviews*, **24**, 107-113. https://doi.org/10.2165/00139709-200524020-00004

[31] Mousaei Sanjerehei, M. (2021) Sample Size Calculations for Vegetation Studies. *Macedonian Journal of Ecology and Environment*, **23**, 85-97. https://doi.org/10.59194/mjee21232085ms

[32] Souza, R.R.d., Toebe, M., Marchioro, V.S., Cargnelutti Filho, A., Bittencourt, K.C., Mello, A.C., *et al.* (2023) Sample Size and Modeling of Plant Variability Using Precision Statistics in Soybean Counting Traits. *Field Crops Research*, **291**, Article 108789. https://doi.org/10.1016/j.fcr.2022.108789

[33] Dikici, B., Saad, H.A.K. and Zhao, B. (2024) Evaluating Flow Characteristics of Ground and Cut Biomass for Industrial Applications. *Powders*, **3**, 437-459. https://doi.org/10.3390/powders3030024

[34] Capareda, S. (2023) Introduction to Biomass Energy Conversions. CRC Press.

[35] Baümler, E., Cuniberti, A., Nolasco, S.M. and Riccobene, I.C. (2006) Moisture Dependent Physical and Compression Properties of Safflower Seed. *Journal of Food Engineering*, **72**, 134-140. https://doi.org/10.1016/j.jfoodeng.2004.11.029

[36] Kibar, H. and Ozturk, T. (2008) Physical and Mechanical Properties of Soybean. *International Agrophysics*, **22**, 239-244. http://agro.icm.edu.pl/agro/element/bwmeta1.element.agro-article-b7af20ac-4f8b-458e-bb66-247eca578e4d

[37] Abdelmoulaa, M., Zaalouk, A. and Mahmoud, W. (2024) Determining Some Physical, Mechanical and Aerodynamic Properties of Chamomile Flowers to Design a Picking Mechanism. *Al-Azhar Journal of Agricultural Engineering*, **7**, 1.

[38] Uba, F., Esandoh, E.O., Zogho, D. and Anokye, E.G. (2020) Physical and Mechanical Properties of Locally Cultivated Tomatoes in Sunyani, Ghana. *Scientific African*, **10**, e00616. https://doi.org/10.1016/j.sciaf.2020.e00616

[39] Rahman Khan, M.M., Chen, Y., Belsham, T., Laguë, C., Landry, H., Peng, Q., *et al.* (2011) Fineness and Tensile Properties of Hemp (*Cannabis sativa* L.) Fibres. *Biosystems Engineering*, **108**, 9-17. https://doi.org/10.1016/j.biosystemseng.2010.10.004

[40] Liu, Q., Mathanker, S.K., Zhang, Q. and Hansen, A.C. (2012) Biomechanical Properties of Miscanthus Stems. *Transactions of the ASABE*, **55**, 1125-1131. https://doi.org/10.13031/2013.42231

[41] Khazaei, J., Rabbani, H., Ebadi, A. and Golbabaei, F. (2003) Determining the Shear Strength and Picking Force for Pyrethrum Flower. *Iranian Journal of Agricultural Sciences*, **33**, 433-444.

[42] Shivashimpar, A., Parray, R.A., Mani, I., Kushwaha, H., Lande, S., Mirzakhaninafchi, H., *et al.* (2023) On-Farm Cropping Sensor-Based Smart Device for Cutting Energy Measurement of Cereal Crops. *Agronomy Journal*, **115**, 2674-2693. https://doi.org/10.1002/agj2.21225

[43] Lubis, A., Mandang, T., Hermawan, W., *et al.* (2021) Study of the Physical and Mechanical Characteristics of Patchouli Plants. *AIMS Agriculture and Food*, **6**, 525-537. https://doi.org/10.3934/agrfood.2021030

[44] Cheng, Z., Leal, J.H., Hartford, C.E., Carson, J.W., Donohoe, B.S., Craig, D.A., *et al.* (2021) Flow Behavior Characterization of Biomass Feedstocks. *Powder Technology*, **387**, 156-180. https://doi.org/10.1016/j.powtec.2021.04.004

[45] de Winter, J.C.F., Gosling, S.D. and Potter, J. (2016) Comparing the Pearson and Spearman Correlation Coefficients across Distributions and Sample Sizes: A Tutorial Using Simulations and Empirical Data. *Psychological Methods*, **21**, 273-290. https://doi.org/10.1037/met0000079

[46] Abdelfattah, E.H. (2024) On Comparing the Power of Weighted and Unweighted Rank Correlation Coefficients. *Advances and Applications in Statistics*, **91**, 895-905. https://doi.org/10.17654/0972361724048

[47] Schober, P., Boer, C. and Schwarte, L.A. (2018) Correlation Coefficients: Appropriate Use and Interpretation. *Anesthesia & Analgesia*, **126**, 1763-1768. https://doi.org/10.1213/ane.0000000000002864

[48] Yu, H. and Hutson, A.D. (2024) A Robust Spearman Correlation Coefficient Permutation Test. *Communications in Statistics—Theory and Methods*, **53**, 2141-2153. https://doi.org/10.1080/03610926.2022.2121144

[49] Ali Abd Al-Hameed, K. (2022) Spearman's Correlation Coefficient in Statistical Analysis. *International Journal of Nonlinear Analysis and Applications*, **13**, 3249-3255.

[50] Temizhan, E., Mirtagioglu, H. and Mendes, M. (2022) Which Correlation Coefficient Should Be Used for Investigating Relations between Quantitative Variables? *American Scientific Research Journal for Engineering, Technology, and Sciences*, **85**, 265-277.

[51] Singh, V. and Singh, A. (2020) Analysis of Agriculture Data Using Principal Component Analysis. *International Journal of Multidisciplinary Research and Development*, **7**, 34-37.

[52] Souza, T. (2025) Principal Component Analysis (PCA). In: *Advanced Statistical Analysis for Soil Scientists*, Springer Nature Switzerland, 43-56. https://doi.org/10.1007/978-3-031-88161-9_4

[53] Jolliffe, I.T. and Cadima, J. (2016) Principal Component Analysis: A Review and Recent Developments. *Philosophical Transactions of the Royal Society A: Mathematical, Physical and Engineering Sciences*, **374**, Article 20150202. https://doi.org/10.1098/rsta.2015.0202

[54] Abdi, H. and Williams, L.J. (2010) Principal Component Analysis. *WIREs Computational Statistics*, **2**, 433-459. https://doi.org/10.1002/wics.101

[55] Myers, R.H., Montgomery, D. and Anderson-Cook, C. (2016) Response Surface Methodology: Process and Product Optimization Using Designed Experiments. 1st Edition, Wiley.

[56] Myhan, R., Markowski, M. and Jachimczyk, E. (2020) A Non-Linear Rheological

Model of Plant Tissues. *Biosystems Engineering*, **190**, 1-10. https://doi.org/10.1016/j.biosystemseng.2019.11.018

[57] Aina, A.M., Harith, H.H., Hashim, N. and Mohamad Shukery, M.F. (2025) Finite Element Modelling of the Mechanical Behavior of Papaya Fruit under Compression. *Postharvest Biology and Technology*, **226**, Article 113565. https://doi.org/10.1016/j.postharvbio.2025.113565

[58] Mohsenin, N.N. (1986) Physical Properties of Plant and Animal Materials: Structure, Physical Characteristics, and Mechanical Properties. Gordon and Breach.

[59] Stroshine, R.L. (2004) Physical Properties of Agricultural Materials and Food Products. https://scholar.google.com/citations?view_op=view_citation&hl=en&user=4pkd0FsAAAAJ&citation_for_view=4pkd0FsAAAAJ:qxL8FJ1GzNcC

[60] Lewicki, P.P. and Pawlak, G. (2003) Effect of Drying on Microstructure of Plant Tissue. *Drying Technology*, **21**, 657-683. https://doi.org/10.1081/drt-120019057

[61] Tuly, S.S., Joardder, M.U.H., Welsh, Z.G. and Karim, A. (2025) A Novel Mechanistic Model for Predicting Shrinkage Kinetics in Plant-Based Foods by Integrating Solid Matrix Mobility and Viscoelasticity. *Journal of Food Engineering*, **387**, Article 112346. https://doi.org/10.1016/j.jfoodeng.2024.112346

[62] Dessie, Y., Amsalu, N., Awoke, B. and Gebeyehu, G. (2025) Floral Diversity, Structural Integrity, and Regeneration Patterns of Endba-Zend Dry Afromontane Forest in Northwestern Ethiopia. *BMC Ecology and Evolution*, **25**, Article No. 49. https://doi.org/10.1186/s12862-025-02387-7

[63] Li, L., Yang, M., Zhu, L., Liu, W., Li, L., Cao, W., *et al.* (2024) The Evolution of Mechanical Properties and Cellular Structure of Apples during Freeze Drying Combined with Hot Air Drying (FD-HAD) Process. *Foods*, **13**, Article 3951. https://doi.org/10.3390/foods13233951

[64] Azadbakht, M., Esmaeilzadeh, E. and Esmaeili-Shayan, M. (2015) Energy Consumption during Impact Cutting of Canola Stalk as a Function of Moisture Content and Cutting Height. *Journal of the Saudi Society of Agricultural Sciences*, **14**, 147-152. https://doi.org/10.1016/j.jssas.2013.10.002

[65] Sreekanta, S., Haaning, A., Dobbels, A., O'Neill, R., Hofstad, A., Virdi, K., *et al.* (2024) Variation in Shoot Architecture Traits and Their Relationship to Canopy Coverage and Light Interception in Soybean (Glycine Max). *BMC Plant Biology*, **24**, Article No. 194. https://doi.org/10.1186/s12870-024-04859-2

[66] Tan, J., Liu, X., Li, Q., Ma, K. and Huang, W. (2024) Variation in Internode Length Patterns: A Data Analysis of Internode Length and Serial Number in Three Bamboo Species. *Frontiers in Ecology and Evolution*, **12**, Article 1440494. https://doi.org/10.3389/fevo.2024.1440494

[67] Wang, F., Yu, Z., Zhang, M., Wang, M., Lu, X., Liu, X., *et al.* (2022) ZmTE1 Promotes Plant Height by Regulating Intercalary Meristem Formation and Internode Cell Elongation in Maize. *Plant Biotechnology Journal*, **20**, 526-537. https://doi.org/10.1111/pbi.13734

[68] Zhao, Z., Li, W., Wang, Y., Jin, M., Tang, W., Li, J., *et al.* (2024) Proteomic Investigation Reveals Molecular Mechanisms of Plant Height Regulation in Foxtail Millet. *Journal of Integrative Agriculture*. https://doi.org/10.1016/j.jia.2024.06.014

[69] Chen, L., Li, K., Mou, X., Liu, Z., Jiang, H., Mabrouk, M., *et al.* (2024) Evaluating the Impact of Moisture Content and Loading Orientation on the Geometrical Characteristics and Mechanical Behavior of Cassava Tubers. *Agronomy*, **14**, Article 2254.

https://doi.org/10.3390/agronomy14102254

[70] Krishnakumar, T., Sajeev, M.S., Pradeepika, C., Namrata, A.G., Sanket, J.M., Jeevarathinam, G., *et al.* (2022) Physical and Mechanical Properties of Cassava (*Manihot esculenta* Crantz) Cultivars: Implications for the Design of Mechanical Peeling Machines. *Journal of Food Process Engineering*, **45**, e13923. https://doi.org/10.1111/jfpe.13923